Evaluation of Low- and Medium-Carbon Nb-Microalloyed Plate Steels for Wind Tower Applications

Keith Taylor, Richard Bodnar and Todd Nelson
SSAB Iowa
1755 Bill Sharp Blvd.
Muscatine, IA 52761
Phone – (563) 381-5785
Fax – (563) 381-5766
email: keith.taylor@ssab.com

Steven Jansto
CBMM-Reference Metals Company
1000 Old Pond Road
Bridgeville, PA 15017
Phone – (412) 759-1057
Fax – (412) 221-7355
email: jansto@referencemetals.com

Henrietta Tsosie, Zhiyong Hu, Sheldon Mostovoy and Philip Nash
Illinois Institute of Technology
10 W 32nd. St., Chicago, IL 60616
Phone – (312) 567-3056
Fax – (312) 567-8875
email: nash@iit.edu

Key words: Controlled Rolled, Normalized Rolled, Normalized, Toughness, Fatigue, Fracture Toughness, Nb-Microalloyed

INTRODUCTION

In North America, steel plates for the primary structural members of wind turbine towers are commonly ordered to ASTM A572/A709 Grade 50 or EN 10025-2 Grade S355 standards. For wind tower sites that may experience low ambient temperatures, the plate specifications often require stringent low temperature Charpy V-notch (CVN) toughness requirements, e.g., 30 ft-lbs at –4°F, 42 ft-lbs at –40°F or 25 ft-lbs at -58°F. If plates are ordered to ASTM A572/A709 Grade 50 standards, a low-carbon HSLA steel is typically employed to meet the specified toughness requirements. However, plates ordered to EN 10025-2 Grade S355 with these low-temperature CVN requirements often specify a requirement for "normalized rolling" (e.g., +N delivery condition). Structural steel plates supplied in the normalized rolling condition require control of the hot rolling process such that the final deformation is accomplished over a temperature range which is intended to produce a microstructure and properties equivalent to that obtained in a normalizing heat treatment. Furthermore, steel plates supplied in the normalized rolling condition are, by definition, required to maintain the specified mechanical properties following a normalizing heat treatment. Based on internal studies conducted by SSAB Americas to evaluate the capability of our typical low-carbon A572/A709 Grade 50 to comply with the normalized rolling definition of EN 10025-2, it was determined that these low-carbon HSLA steels, which achieve their excellent balance of strength and toughness principally via ferrite grain refinement and a reduced carbon level, did not have sufficient capability to retain the specified tensile properties after normalizing, as exhibited in Figure 1. Based on these results as well as similar studies, it was determined that in order to comply with the EN 10025-2 normalized rolling definition, a medium-carbon steel must be employed to ensure that the specified minimum as-rolled mechanical properties are retained after normalizing. This paper reports on a collaborative investigation which compares these alternate approaches, viz. low C-Nb controlled rolled steel, a medium C-Nb normalized rolled steel and furnace-normalized medium C-Nb steel. The evaluation includes microstructural characterization, tensile properties, impact toughness, fracture toughness and uniaxial fatigue. A review of available data on fracture toughness and fatigue properties of structural steels similar to those investigated here revealed a surprising lack of such data. Therefore, the authors hope that the information reported here will be useful to the wind turbine design community.

MATERIALS AND PROCEDURES

Steel Selection and Processing. Two basic steel compositions, both suitable for wind tower applications, were selected for this investigation. One is a low-carbon grade (0.06% C) with an addition of about 0.03% Nb. The other is a medium-carbon grade (0.15% C) with an addition of about 0.02% Nb. Henceforth, these steels are referred to as "Low C-Nb" and "Medium C-Nb", respectively. Steel samples were obtained from production plates produced at SSAB Americas' facility in Mobile, AL. Mobile employs a fine grain practice, with a low sulfur content and calcium treatment for sulfide inclusion shape control. Cast slabs 6 inches in thickness were reheated to a temperature sufficiently high to dissolve all of the Nb. Plates were rolled to a final thickness of about 0.75 inches. The rolling temperatures were controlled to produce final microstructures consisting of a mixture of fine polygonal ferrite grains and pearlite.

In addition to the samples from as-rolled plates, a Medium C-Nb plate that had been normalized at 1,650°F was also sampled for evaluation. This steel will be referred to as "Medium C-Nb Normalized" or "Medium C-Nb Norm".

The results of a product chemical analysis on each production plate are provided in Table I. This table also includes the calculated carbon equivalent (CE). The carbon content and carbon equivalent values place the Low C-Nb steel in Zone I of the Graville weldability diagram[1] (Figure 2), while the Medium C-Nb steels fall within Zone II. Although weldability was not investigated in this work, the Low C-Nb steel can be expected to have better weldability than the Medium C-Nb steels.

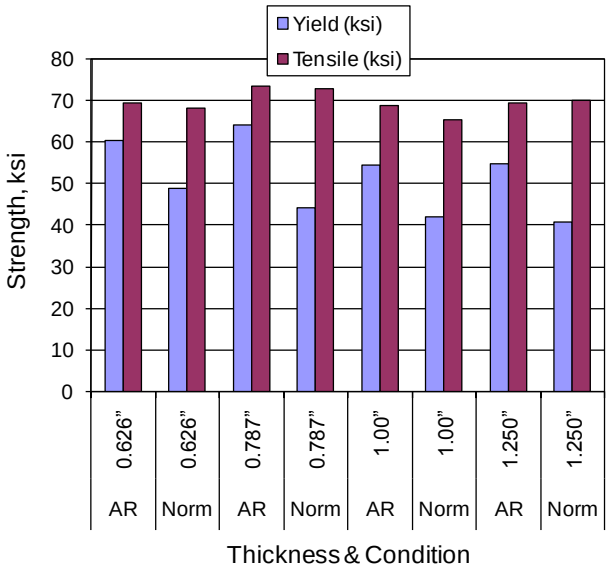

Figure 1. Comparison of tensile properties of as-rolled vs. normalized Low C-Nb HSLA steels (A572-50) of various thicknesses. Normalizing generally results in yield strengths that are below the required minimum of 50 ksi.

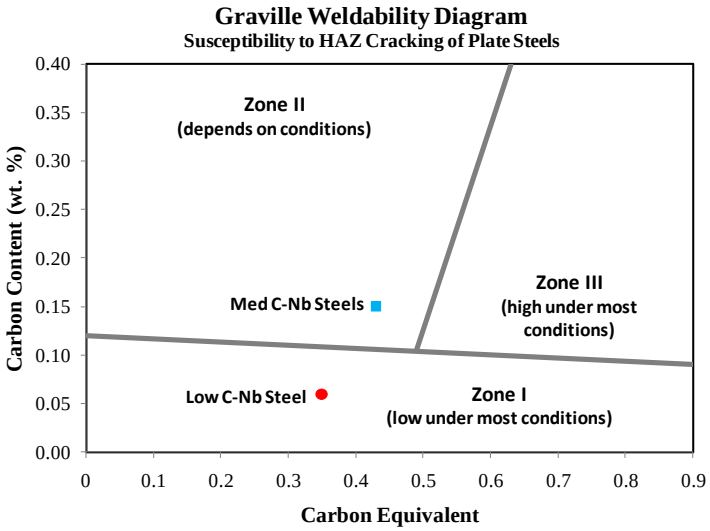

Figure 2. Graville weldability diagram.

Table I. Steel Compositions (wt. %)

Steel	C	Mn	P	S	Si	Cu	Ni+Cr+Mo	Nb	CE[1]
Low C – Nb	0.06	1.27	0.011	0.001	0.34	0.27	0.41	0.031	0.35
Med C – Nb	0.15	1.39	0.012	0.003	0.22	0.20	0.32	0.019	0.43
Med C – Nb Norm	0.15	1.32	0.011	0.003	0.21	0.22	0.23	0.014	0.42
ASTM A572-50 & A709-50 (max)	0.23	1.35	0.04	0.05	0.40	-	-	-	-
EN 10025-2 S355K2 (max)	0.23	1.70	0.035	0.035	0.60	0.60	-	-	0.45
[1]CE = C+Mn/6+(Cr+Mo+V)/5+(Ni+Cu)/15									

Metallography. Specimens for light optical microscopy and scanning electron microscopy were prepared using conventional methods. Longitudinal cross-sections were examined in the as-polished condition for inclusion evaluation as well as after etching with 2% nital. The inclusion content of each steel was determined in accordance with ASTM E2142, Method 1[2]. Specimens were examined in a light optical microscope as well as in Zeiss Ultra 55 and Zeiss EVO/MA10 scanning electron microscopes (SEMs).

Tensile and Impact Toughness Testing. Full-thickness rectangular tensile and CVN impact toughness specimens were prepared in both the longitudinal and transverse orientations and tested in accordance with ASTM E8[3] and E23[4]. The Charpy specimens were machined from the plate quarter-thickness. Charpy specimens for the Medium C-Nb steels were full-size (10 x10mm) while those for the Low C-Nb steel were ¾-size (10 x 7.5mm), in anticipation of higher absorbed energies. The test results for the Low C-Nb steel were converted to a "full-size equivalent" (FSE) value by multiplying by 4/3. CVN testing was conducted at various temperatures from room temperature down to -100°F.

Fracture Toughness Testing. Compact specimens for room-temperature single-specimen fracture toughness testing (J-integral) were prepared and tested in accordance with ASTM E1820[5]. These specimens were machined in a T-L orientation and were 0.75 inches thick (essentially full plate thickness) with integral slots for the displacement gauge attachment (Figure 3). Specimens were fatigue pre-cracked in a closed-loop machine under load control with R = 0.1. The maximum load was about 6 kip at the onset of pre-cracking, and was reduced to about 4 kip as the target pre-crack length of 0.9 inches was reached. Side grooves 0.0375 inches in depth were machined on the pre-cracked specimens. Testing was conducted with a CGS/Lawrence Instron Scientific Corp. model 8500R closed-loop machine controlled by MTS Multi-Purpose TestWare software. An example of the data that is collected by this program is shown in Figure 4. The data collected are: 1) displacement (crosshead extension), 2) strain (the displacement recorded by clip gage), and 3) load. The program runs through a simple set of repetitions as outlined below.

1) Pre-load and unload five times to determine an average unloading compliance of the pre-cracked specimen.
2) Allow the machine to ramp for 10 minutes or to a destination of 1 inch, without exceeding the upper limit incremental of 0.005 inches (beginning at 0.01 inches).
3) Once the upper limit is tripped, hold at displacement (crosshead extension) for 5 minutes to allow for load relaxation.
4) Unload to a negative displacement of 0.1 inches without exceeding a lower limit of 0.005 inches (upper limit minus 0.005 inches).
5) Once the lower limit is tripped, the process begins again with an increased displacement which is determined by the user while maintaining ASTM E1820 requirements.

This procedure is repeated several times to obtain a J-Δa curve. Once the program has completed, the specimen is heat-tinted by placing on a hot plate for at least 5 minutes or until the specimen turns blue. The specimen is then fractured by fatiguing in a closed-loop machine.

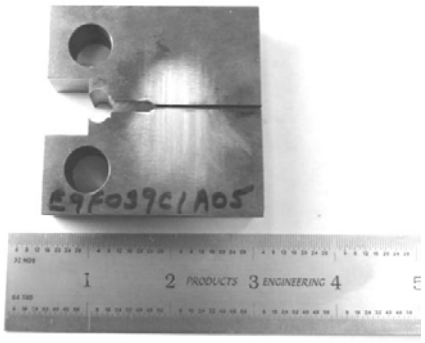

Figure 3. Compact specimen for fracture toughness testing.

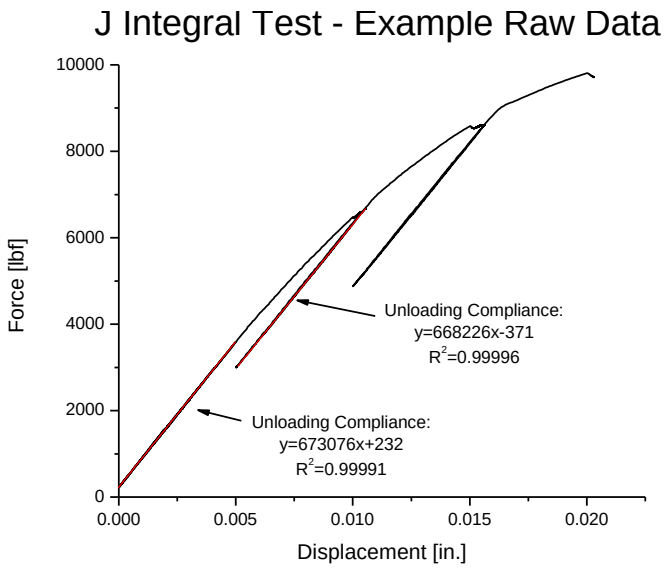

Figure 4. Example of J-integral test data.

For each specimen, several incremental measurements of initial crack length and final crack length are made using a comparator. The total thickness (B) and side-grooved thickness (B_N) are measured using the comparator as well. The results of each test provide information to determine unloading compliances, J elastic and plastic areas. The ASTM analysis allows the value J_Q to be determined using a set of offsets and curve fits. For the value of J_Q to be considered J_{Ic}, the width of the specimen and the initial ligament (b_o) must meet the following requirement:

$$B \& b_o > 25\frac{J_Q}{\sigma_Y} \qquad (1)$$

where σ_Y is the effective yield strength (i.e., the average of the UTS and 0.2% offset yield strength as determined from a tensile test).

The relationship between J_{Ic} and K_{Ic} for plane strain conditions is:

$$J_{Ic} = K_{Ic}^{2}\left(\frac{1-\nu^{2}}{E}\right) \qquad (2)$$

Where ν is the Poisson's ratio and E is the Young's modulus (assumed to be 0.3 and 29,000 ksi, respectively).

Uniaxial Fatigue Testing. Specimens for fatigue testing were prepared and tested in accordance with ASTM E466[6]. Hourglass specimens with a diameter of 0.3 inches (Figure 5) were machined from the plate mid-thickness in a transverse orientation. All machining marks were removed by finishing the reduced section starting with an appropriate grit size and finishing with 600 grit sandpaper. Care was taken to ensure that all transverse machining marks were removed from the reduced section of the test specimens. A laser micrometer was used to measure the final specimen diameter (average of three measurements). Fully reversed (R = -1) load-controlled fatigue testing was carried out with an MTS 880 testing machine (Figure 6). A fan was suspended from the upper specimen clamp to minimize specimen heating during testing. Specimens were tested at alternating stresses (S_a) up to about 54 ksi at a frequency of 4Hz, except at stress levels near the endurance limit (S_e) when a frequency of 8Hz or 10Hz was used. Three different tests were conducted at each alternating stress level. Testing was carried out until failure or when 10^7 cycles was reached.

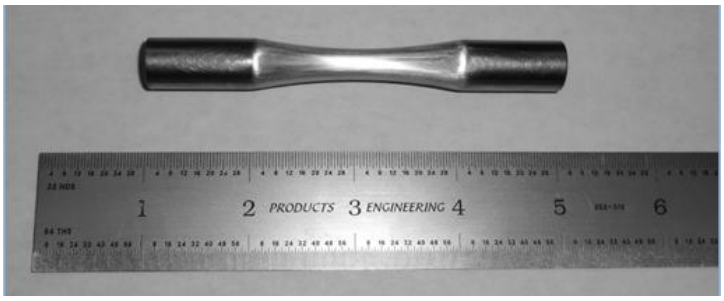

Figure 5. Typical fatigue test specimen.

Figure 6. Fatigue testing setup.

RESULTS

Metallography. The results of inclusion analysis are summarized in Table II. Overall, the internal cleanliness of each steel is very good. Because of the low sulfur contents of these steels, essentially no Type A elongated MnS inclusions were detected in the SEM-based analysis. However, close inspection revealed the presence of very thin MnS inclusions in both of the Medium C-Nb steels, especially near the mid-thickness (Figure 7). In contrast, the extremely low sulfur content of the Low C-Nb steel (0.001%) resulted in essentially no elongated MnS inclusions. Each steel contains a dispersion of spheroidal Type D oxysulfide inclusions containing calcium and aluminum, an example of which is shown in Figure 8. The Low C-Nb steel exhibits a somewhat greater number of these inclusions than the Medium C-Nb steels.

Table II. Inclusion Analysis Results

	Sulfide A		Alumina B		Silicate C		Globular D	
Steel	**Thin**	**Heavy**	**Thin**	**Heavy**	**Thin**	**Heavy**	**Thin**	**Heavy**
Low C-Nb	0.00	0.00	0.50	0.00	0.00	0.00	1.50	0.50
Medium C-Nb	0.00	0.00	0.00	0.00	0.00	0.00	1.00	0.00
Medium C-Nb Norm	0.00	0.00	0.00	0.00	0.00	0.00	0.50	0.50

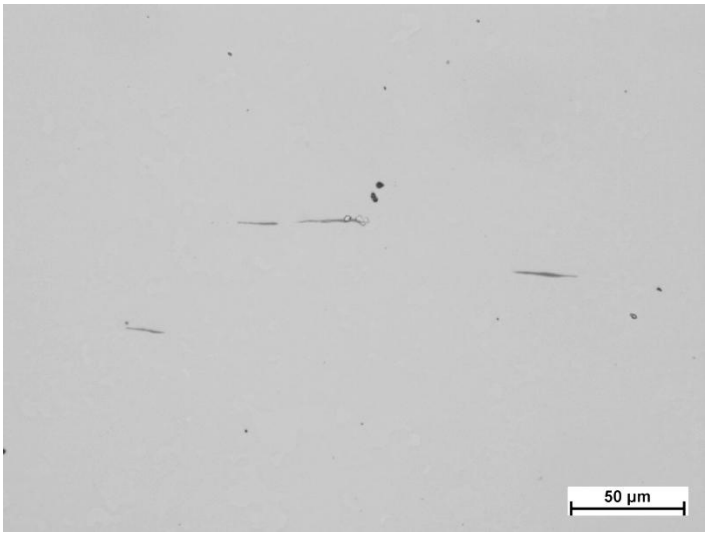

Figure 7. MnS inclusions in the Medium C-Nb Norm steel.

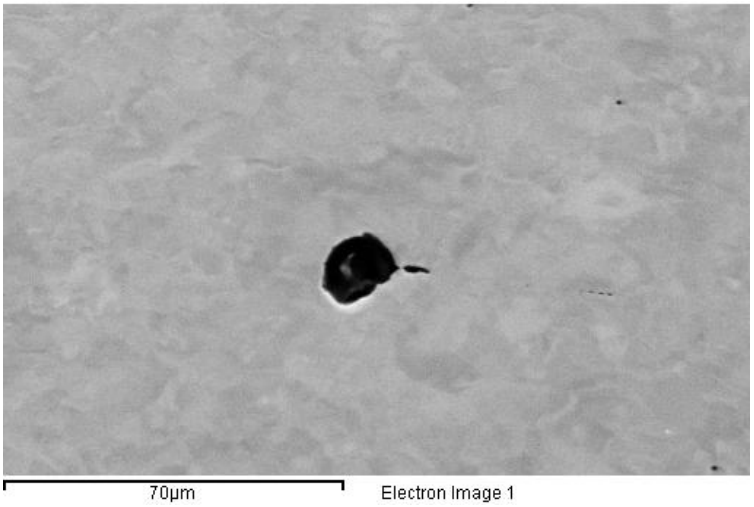

Figure 8. A typical Ca-Al oxysulfide inclusion (Low C-Nb steel).

Figures 9a-9c show light-optical and SEM images of etched metallographic cross sections. All microstructures consist predominantly of a mixture of polygonal ferrite and pearlite. In each case, the ferrite grain size (mean grain diameter) is about 7m. The Low C-Nb steel contains about 7% pearlite while both of the Medium C-Nb steels contain about 28% pearlite in a banded distribution.

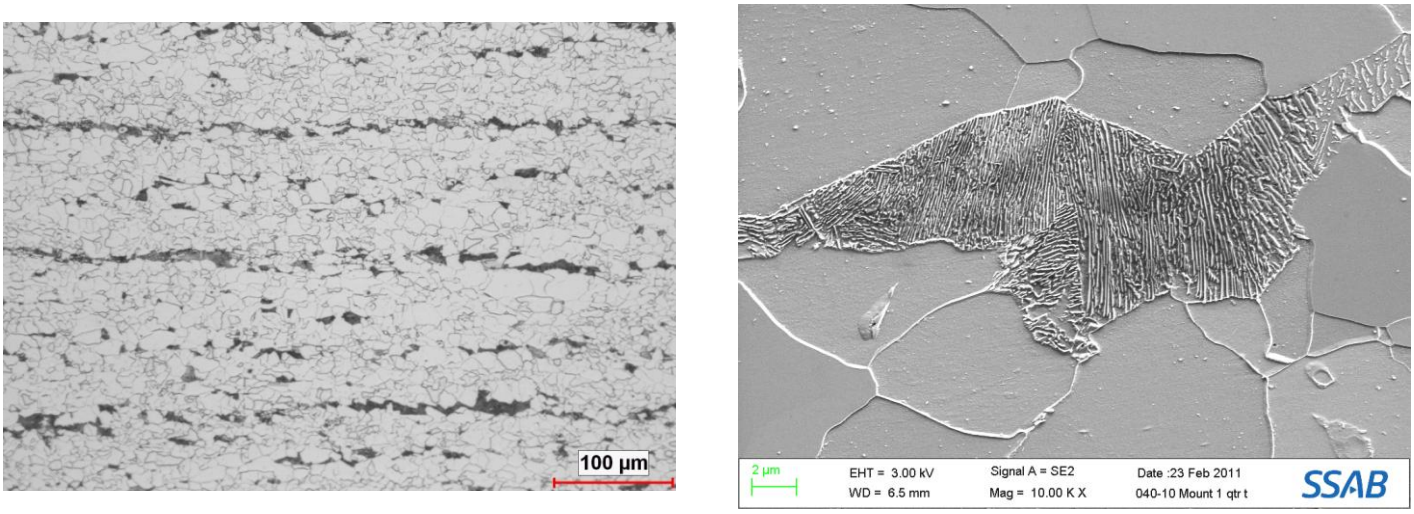

Figure 9a. Microstructure of the Low C-Nb steel (light-optical (left) and SEM secondary electron images (right)). The microstructure is predominantly a mixture of polygonal ferrite and pearlite. The mean ferrite grain diameter is about 7.2m and the pearlite content is about 7%.

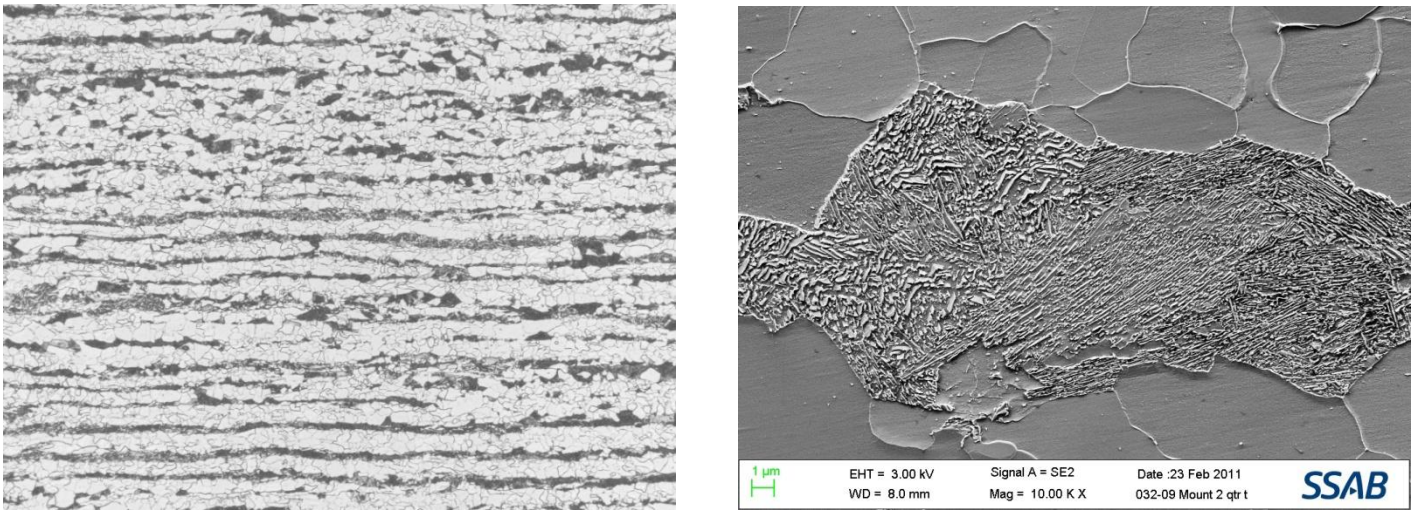

Figure 9b. Microstructure of the Medium C-Nb steel (light-optical (left) and SEM secondary electron images (right)). The microstructure is predominantly a mixture of polygonal ferrite and pearlite. The mean ferrite grain diameter is about 6.7m and the pearlite content is about 28%.

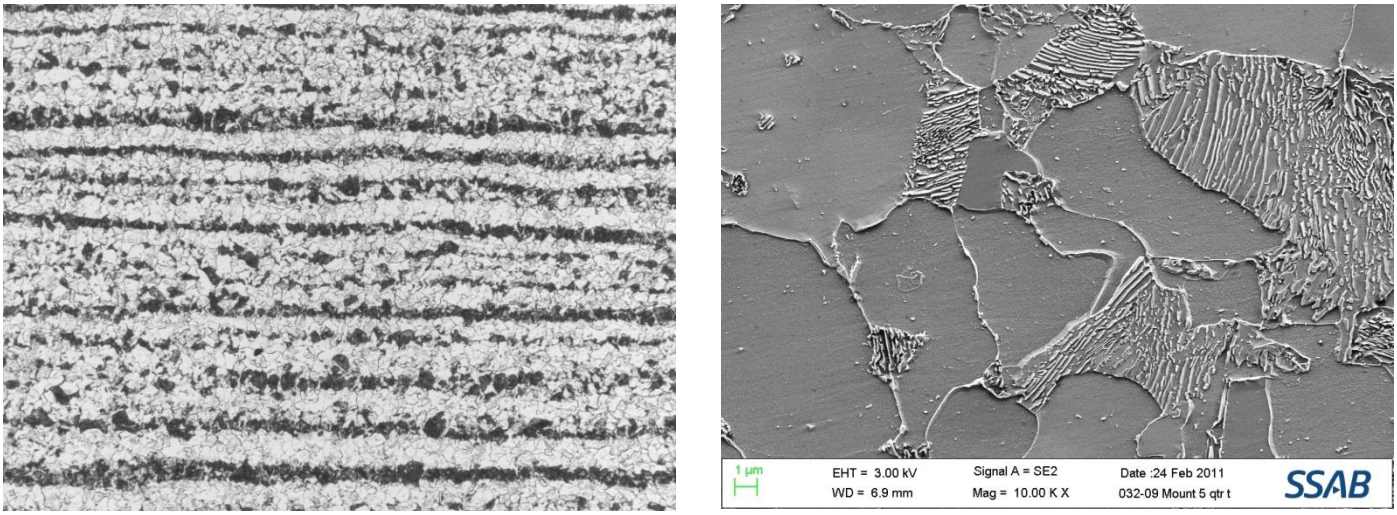

Figure 9c. Microstructure of the Medium C-Nb Normalized steel (light-optical (left) and SEM secondary electron images (right)). The microstructure is predominantly a mixture of polygonal ferrite and pearlite. The mean ferrite grain diameter is about 7.4m and the pearlite content is about 27%.

Tensile Properties and Impact Toughness. Tensile properties and Charpy absorbed energy at a test temperature of -60°F are provided in Table III. A temperature of -60°F is about the lowest test temperature for which designers of wind turbine towers have a toughness requirement. Overall, the tensile properties of each steel are similar for both test orientations. The as-rolled steels have similar yield strength of about 63 to 65 ksi. The tensile strength of the Low C-Nb steel is about 75 ksi while that for the Medium C-Nb steel is about 82 ksi. The most notable difference between these as-rolled steels is the impact toughness. The -60°F absorbed energies for the Low C-Nb steel are over 250 ft-lbs, while values for the Medium C-Nb steel are less than 100 ft-lbs. The Low C-Nb steel also exhibits less toughness anisotropy (i.e., a smaller energy difference between longitudinal vs. transverse test orientations), presumably due to its lower sulfide-inclusion content.

Normalizing decreases the yield strength of the Medium C-Nb grade from about 64 to about 56 ksi, and decreases the tensile strength from about 82 to about 77 ksi. A substantial increase in Charpy absorbed energy is gained by the normalizing treatment, presumably due to a strength-toughness tradeoff.

Figure 10 plots CVN energy for each steel vs. test temperature for transverse and longitudinal orientations. The superior toughness of the Low C-Nb steel is readily apparent, with upper shelf behavior extending to temperatures as low as about -60°F. It should be noted that each steel meets the tensile and Charpy requirements of the ASTM and EN specifications by comfortable margins (see Table III).

Fracture Toughness. Three individual tests were run for each steel and the results are summarized in Figures 11 through 13. The results for the tests are valid for K_{Ic} calculation with the exception of one of the tests on the Low C-Nb steel. The Low C-Nb steel exhibits K_{Ic} levels of about 350 and 400 ksi/in. while values for the Medium C-Nb steels are in the range of about 215 to 290 ksi/√in.

Table III. Tensile and -60°F CVN Results.

Steel	Orientation	YS (ksi)	UTS (ksi)	El. in 8" (%)	CVN @ -60°F (ft-lbs)
Low C – Nb	L	63.3	74.5	29.7	283 [1]
	T	65.2	75.6	28.1	274 [1]
Med C – Nb	L	63.6	81.3	21.9	76
	T	64.1	82.5	23.3	31
Med C – Nb Normalized	L	55.7	76.5	28.3	179
	T	56.7	76.8	27.6	97
ASTM A572-50 & A709-50		50 min	65 min	18 min	25 min LCVN @ 10°F [2]
EN 10025-2 S355K2[3]		50 min	68 - 91	20 min	30 min LCVN @ -4°F

[1] Full-Size Equivalent
[2] ASTM A709 requirement for Zone 3 fracture critical tension components
[3] $16 < t \leq 40$mm

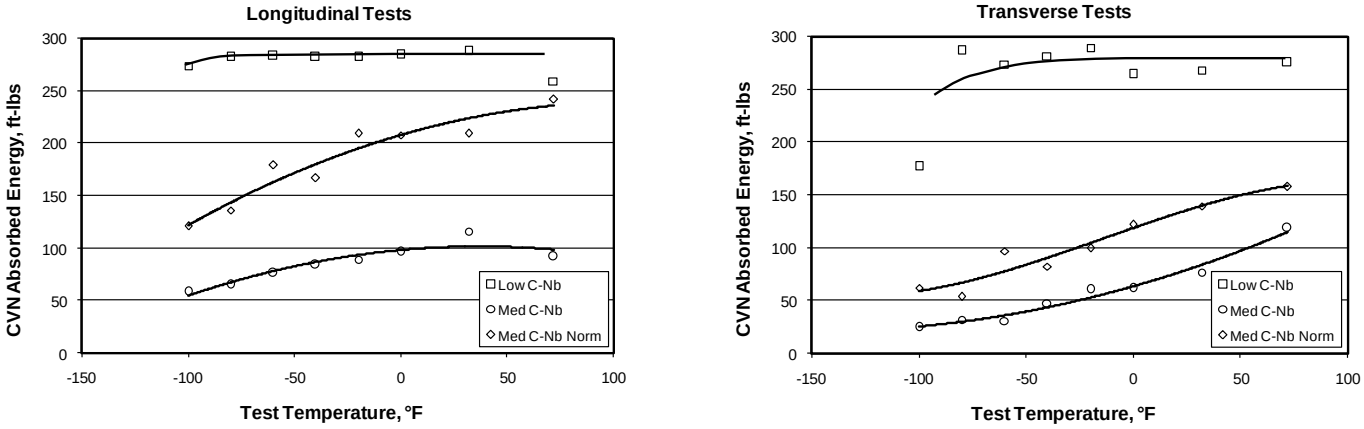

Figure 10. Charpy absorbed energy vs. test temperature.

Uniaxial Fatigue. Figures 14 through 16 plot alternating stress vs. cycles to failure for each of the steels. These figures also show linear fits to the individual data points. A complete S-N curve was developed for each steel by suitable selection of an endurance limit based on the runout test results. These S-N curves are plotted together in Figure 17 to facilitate comparison of the fatigue life behavior. Based on the results, endurance limits for the three steels are as follows: Low C-Nb – 44 ksi; Medium C-Nb – 39 ksi; Medium C-Nb Normalized – 35 ksi. In general, fatigue crack initiation occurred at the specimen surface (Figure 18), as expected.

DISCUSSION

Table IV provides a summary of the mechanical properties (transverse) of the steels evaluated in this investigation. Values for K_{Ic} represent the average of the two or three valid test results reported earlier. As mentioned in the Introduction, available fracture toughness data is limited for structural steels similar to those examined in this study. However, Wilson[7] has investigated the fracture properties of a low-sulfur (0.003%) ASTM A588 Grade A steel. The A588 steels have mechanical properties and chemistry similar to the current Medium C-Nb steels, except that Grade A is microalloyed with vanadium instead of niobium. Wilson reported a fracture toughness of 420 ksi/√in for the A588 steel, but the J-integral test was not valid for a K_{Ic} determination. A valid test would presumably have produced a lower result, perhaps close to the 235 and 250 ksi/in. of the current Medium C-Nb steels. In any case, the Low C-Nb steel with a K_{Ic} of about 375 ksi/in. clearly has superior fracture toughness as compared to the Medium C-Nb steels. This higher toughness can be attributed to its lower pearlite and sulfide-inclusion contents.

A somewhat surprising result of this investigation concerns the higher endurance limit of the Low C-Nb steel as compared to the Medium C-Nb steels. Typically, the fatigue endurance limit is expected to correlate with tensile strength, and the Low C-Nb steel has a somewhat lower tensile strength than the Medium C-Nb steels. The lower sulfide-inclusion content may contribute to the improved fatigue resistance of the Low C-Nb steel. The endurance limit for the Low C-Nb steel, 44 ksi, is similar to that reported by Chen, et. al.[8] for an ASTM A709 Grade 70 steel.

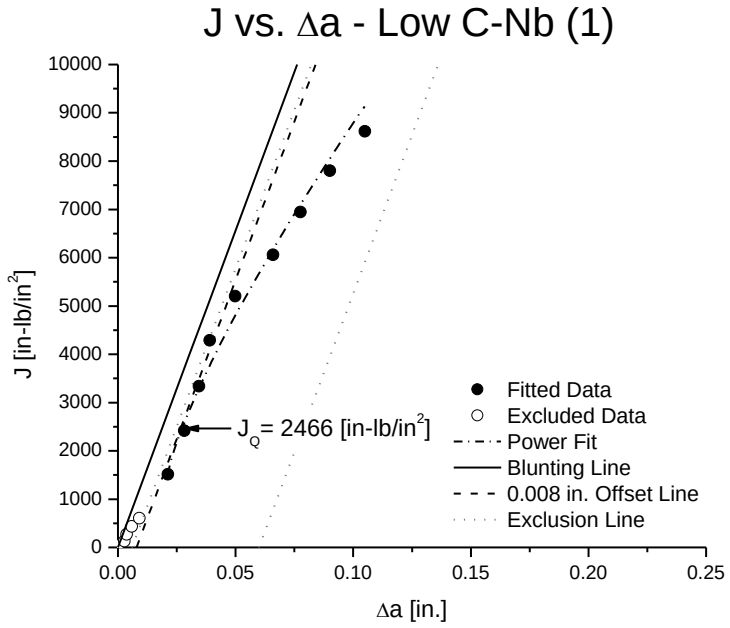

Specimen	Measured a_o [in.]	Measured a_f [in.]	Calculated a_o [in.]	Calculated a_f [in.]	%Diff		%Error		J_Q [in-lb/in^2]	$25(J_Q/\sigma_Y)$	Valid?	K_{Ic} [ksi/√in]
1	0.95	1.04	0.93	1.03	8.1	3.0	1.8	0.8	2466	0.94	Yes	399
2	0.93	1.02	0.90	1.03	11.1	3.6	2.6	1.3	1912	0.73	Yes	351
3	0.95	1.05	0.92	1.02	9.3	0.7	3.0	3.0	3124	1.19	No	---

Figure 11. Fracture toughness results for the Low C-Nb steel: an example of a J-Δa plot and a tabular summary of the test data.

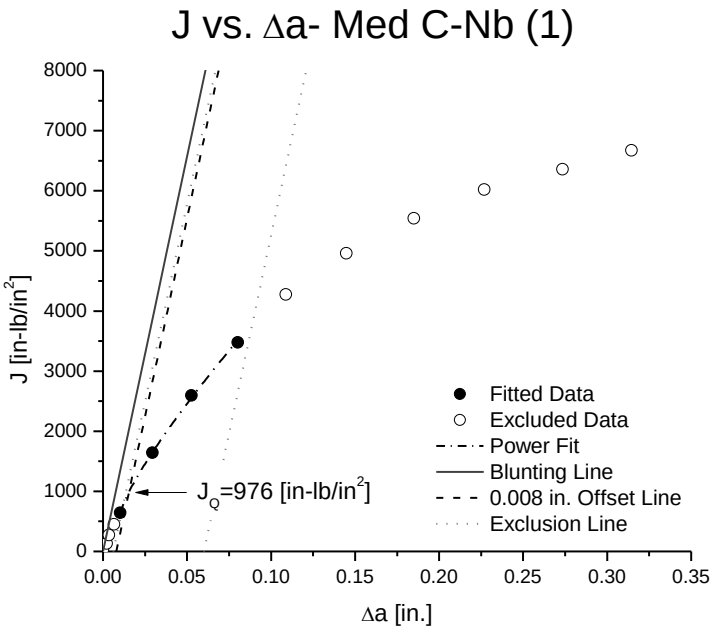

Specimen	Measured a_o [in.]	Measured a_f [in.]	Calculated a_o [in.]	Calculated a_f [in.]	%Diff		%Error		J_Q [in-lb/in^2]	$25(J_Q/\sigma_Y)$	Valid?	K_{Ic} [ksi/√in]
1	0.95	1.29	0.92	1.24	8.8	22.1	2.5	3.6	976	0.37	Yes	251
2	0.94	1.28	0.92	1.23	9.2	21.5	2.3	3.7	741	0.28	Yes	219
3	0.96	1.27	0.94	1.23	6.5	21.2	1.7	3.4	875	0.33	Yes	238

Figure 12. Fracture toughness results for the Medium C-Nb steel: an example of a J-Δa plot and a tabular summary of the test data.

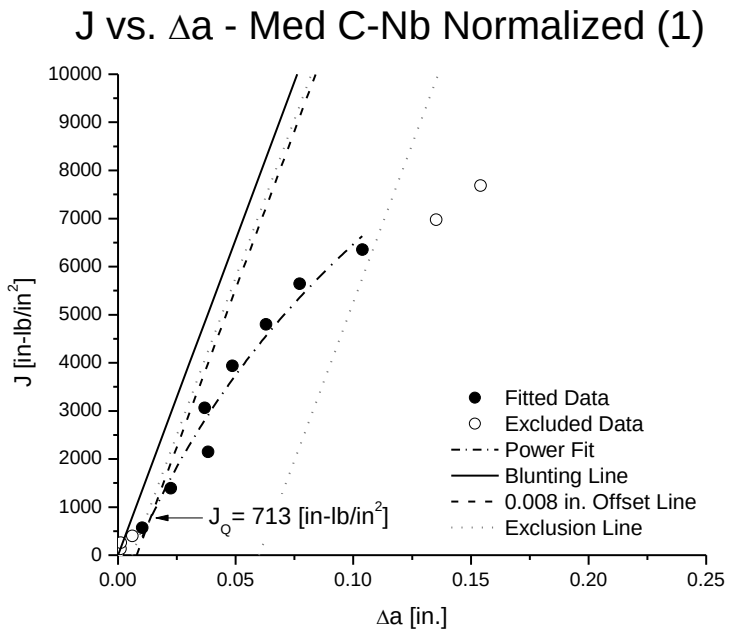

Specimen	Measured a_o [in.]	Measured a_f [in.]	Calculated a_o [in.]	Calculated a_f [in.]	%Diff		%Error		J_Q [in-lb/in^2]	$25(J_Q/\sigma_Y)$	Valid?	K_{Ic} [ksi/√in]
1	0.90	1.12	0.92	1.07	7.1	5.0	2.3	4.3	713	0.27	Yes	215
2	0.92	1.19	0.92	1.07	7.9	1.8	0.3	10.1	1294	0.49	Yes	289
3	0.94	1.16	0.92	1.07	8.6	2.7	1.7	7.8	924	0.35	Yes	244

Figure 13. Fracture toughness results for the Medium C-Nb Normalized steel: an example of a J-Δa plot and a tabular summary of the test data.

To understand the differences in fatigue endurance limits of the current steels, it is useful to consider the different strengthening mechanisms at play in these steels. Strengthening mechanisms that pertain to these steels are the lattice strength of iron (base strength), solid-solution strengthening, pearlite strengthening, ferrite grain size (FGS) strengthening, and precipitation strengthening. It is possible to estimate the contributions of these strengthening mechanisms by referring to the literature and utilizing quantitative metallography results[9]. Consider the empirical regression equation for yield strength of C-Mn steels developed by Grozier and Bucher[10]:

$$YS_{calc}\ (ksi) = 13.3 + 5.9(\%Mn) + 10.2(\%Si) + 0.22(\%Pearlite) + 2.4(1/\sqrt{d}), \qquad (3)$$

where d is the ferrite grain size in mm. The constant, 13.3 ksi, represents the base or lattice strength of iron. Mn and Si contribute to solid-solution strengthening. Irvine and Pickering[11] considered additional solid-solution elements and proposed the following coefficients for the elements Mn, Si, Cu, Mo, Ni, and Cr: +4.7, +12.2, +12.2, +2.0, 0, and –4.5 ksi/wt. %, respectively. The Mn and Si coefficients for solid-solution strengthening of Irvine and Pickering are similar to those of Grozier and Bucher.

The yield strength contributions from solid-solution strengthening vary between about 11 and 13 ksi for the present steels. The contribution of pearlite to strengthening is minimal for the Low C-Nb steels, but is about 6 ksi for the Medium C-Nb steels. Grain size strengthening is similar in all steels, at 28 to 29 ksi. Of the various strengthening mechanisms, that due to precipitation of Nb(C,N) is expected to show the largest variation among the present steels. This strengthening increment can be inferred from the difference between YS_{calc} and the measured yield strength, i.e.,

$$\Delta YS_{Nb(C,N)} = YS_{meas.} - YS_{calc} \qquad (4)$$

Figure 19 shows the individual contribution of each mechanism to the yield strength of each steel. It is evident that Nb(C,N) precipitation contributes substantially (by about 10 ksi) to the yield strength of the Low C-Nb steel, modestly (by 3.6 ksi) to that of the Medium C-Nb steel, and makes essentially no contribution to the yield strength of the normalized steel. Precipitation in the Low C-Nb steel occurs during plate rolling and subsequent cooling, but at temperatures low enough that precipitate coarsening is limited. The

Medium C-Nb steels have lower Nb contents, and this is part of the reason that the precipitation strengthening increments are smaller. The higher carbon content of the Medium C-Nb steels also results in precipitation at higher temperatures with attendant precipitate coarsening. In the normalized steel, further coarsening takes place during heat treatment. It is speculated that Nb(C,N) precipitates contribute to cyclic strain hardening during fatigue testing, and that this cyclic hardening contributes to the higher fatigue life and endurance limit of the Low C-Nb steel as compared to the Medium C-Nb steels.

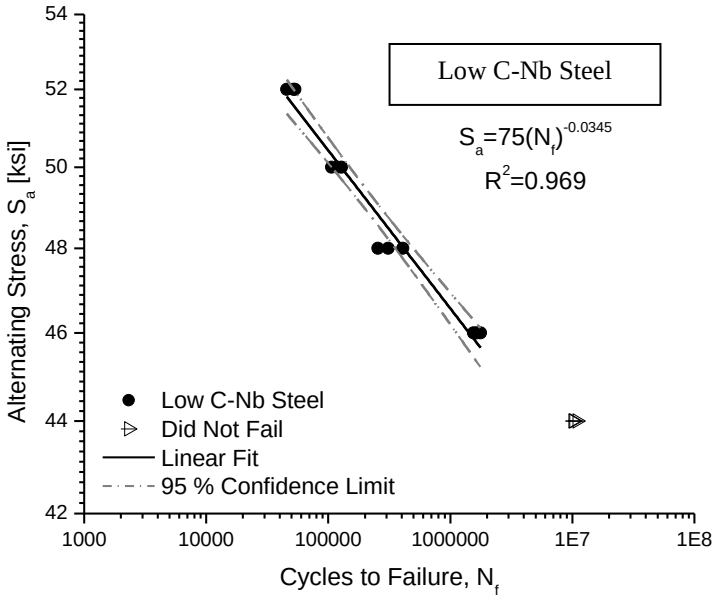

Figure 14. S-N curve for the Low C-Nb steel.

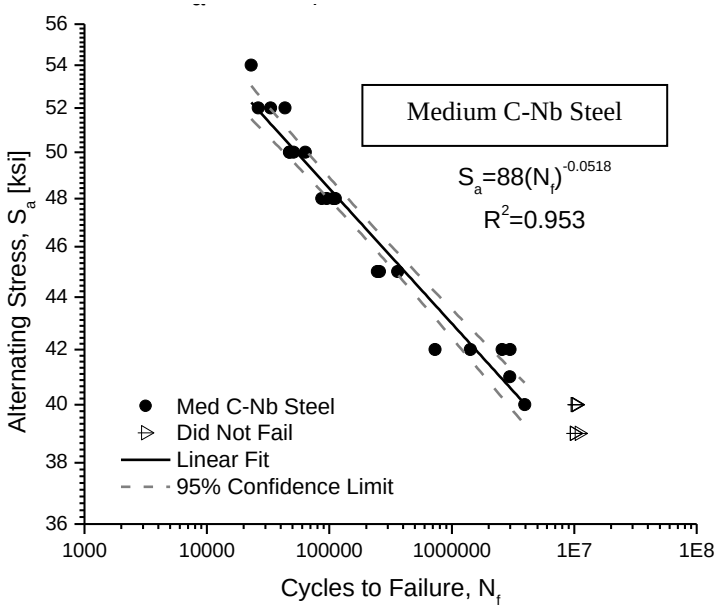

Figure 15. S-N curve for the Medium C-Nb steel.

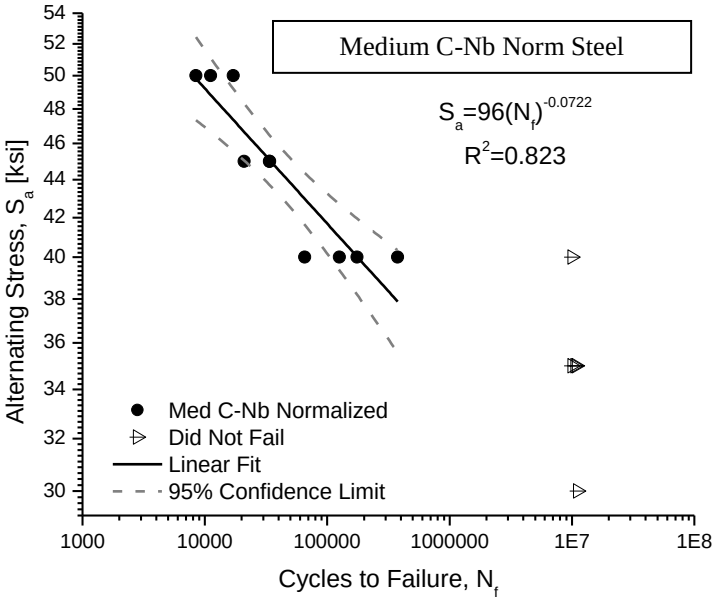

Figure 16. S-N curve for the Medium C-Nb Normalized steel.

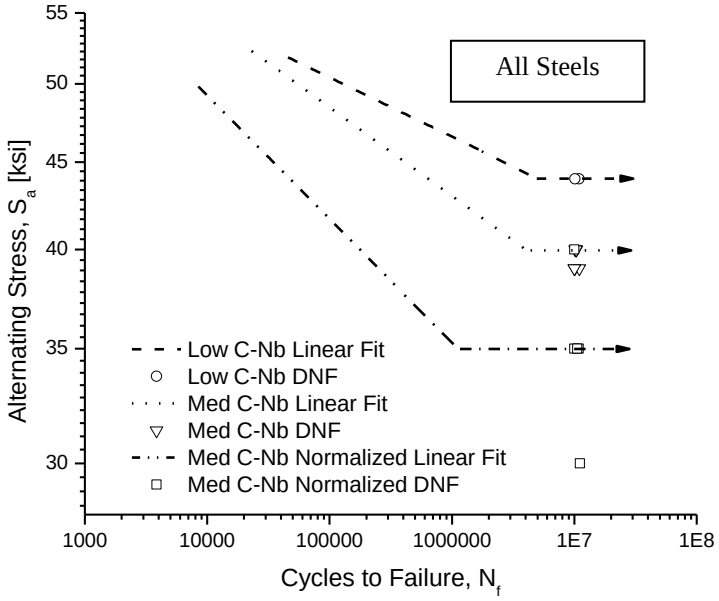

Figure 17. Fitted S-N curves for all of the steels.

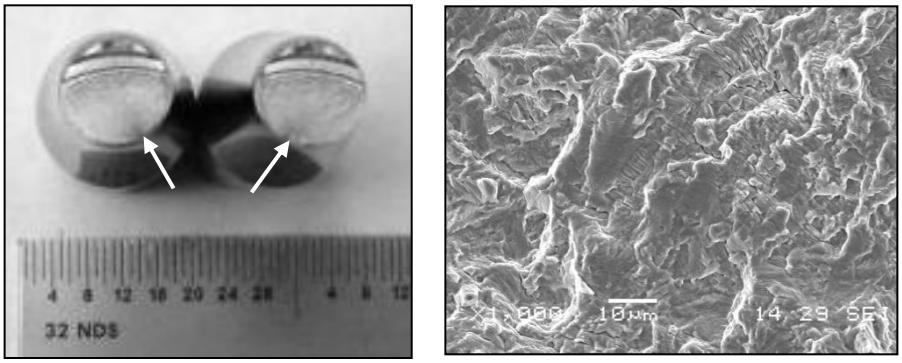

Figure 18. Fatigue crack initiation consistently took place on the specimen surface (arrow) with ductile crack propagation.

Table IV. Mechanical Property Summary

Steel	YS (ksi)	UTS (ksi)	-60°F TCVN (ft-lbs)	Upper Shelf TCVN (ft-lbs)	Fracture Toughness, K_{Ic} (ksi/√in)	Fatigue Endurance Limit, S_e (ksi)
Low C – Nb	65	76	270	280	375	44
Medium C – Nb	64	82	30	120	235	39
Medium C – Nb Normalized	57	77	80	160	250	35

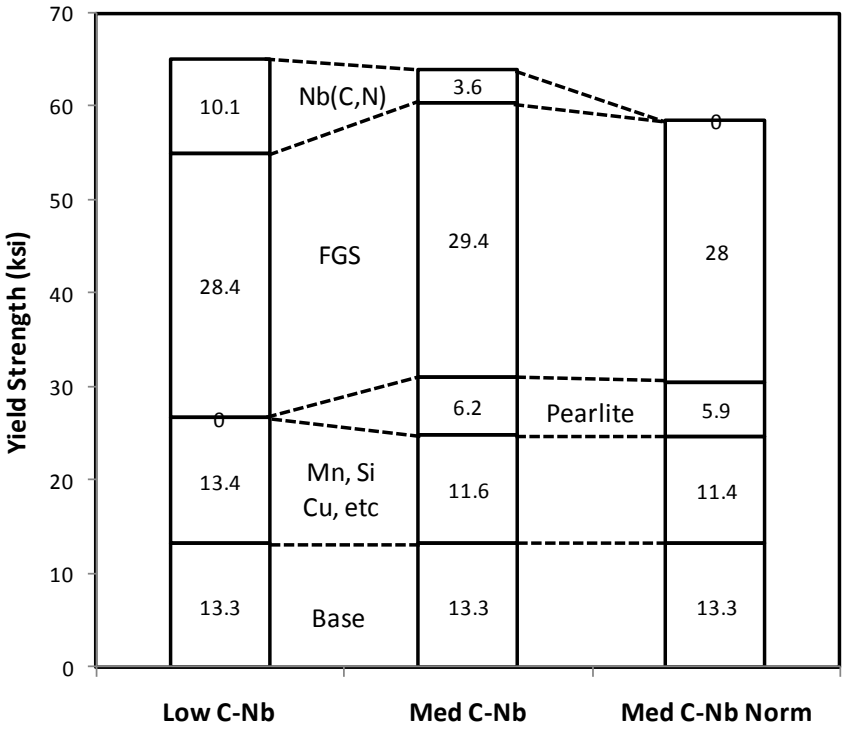

Figure 19. Contributions to yield strength for the various strengthening mechanisms.

It is generally known that fatigue cracks in polished specimens initiate due to damage to persistent slip bands at the specimen surface[12]. In ferrite-pearlite steels, the damage generally occurs in the ferrite as opposed to the pearlite, which can arrest cracks from propagating[13]. Ferrite which has been more effectively strengthened by Nb(C,N) precipitates (e.g., Low C-Nb steel) will exhibit greater cyclic hardening[14]. This greater cyclic hardening provides more resistance to slip, thereby leading to a higher fatigue endurance limit. Others have also observed cyclic hardening and excellent fatigue strength in microalloyed steels[15-17].

CONCLUSION

This investigation has shown that controlled rolled low-carbon Nb-microalloyed steels offer considerable advantages to wind turbine tower producers in the form of improved impact toughness and fracture toughness as compared to medium-carbon steels. The toughness benefit is attributed primarily due to the lower, more uniformly distributed pearlite content of low-carbon steels. Precipitation of Nb(C,N) provides a substantial contribution to yield strength in low-carbon steels, which also appears to improve fatigue resistance perhaps due to a cyclic strain hardening mechanism. Based on these results, the implications of specifying the EN 10025 normalized rolling delivery condition are clear: the steel chemical composition constraints imposed by the EN 10025 normalized rolling requirement result in wind turbine tower plates with reduced weldability, toughness and fatigue resistance.

The authors plan to conduct additional fracture toughness testing at -40°F, as well as room-temperature fatigue crack growth testing. The results of this additional testing will be reported at a later date.

ACKNOWLEDGEMENTS

We gratefully acknowledge the assistance from Scott Smith with the tensile and Charpy testing, Eric Gilbertson with the scanning electron microscopy and Justin Raines with the inclusion analysis.

REFERENCES

1. B.A. Graville, "Cold Cracking in Welds in HSLA Steels," *Welding of HSLA (Microalloyed) Structural Steels*, ASM, Metals Park, OH, 1976.
2. ASTM Standard E2142, "Test Methods for Rating and Classifying Inclusions in Steel Using the Scanning Electron Microscope," *Annual Book of ASTM Standards*, vol. 03.01, ASTM International, Conshohocken, PA, 2010.
3. ASTM Standard E8, "Test Methods for Tension Testing of Metallic Materials," *Annual Book of ASTM Standards*, vol. 03.01, ASTM International, Conshohocken, PA, 2010.
4. ASTM Standard E23, "Test Methods for Notched Bar Impact Testing of Metallic Materials," *Annual Book of ASTM Standards*, vol. 03.01, ASTM International, Conshohocken, PA, 2010.
5. ASTM Standard E1820, "Test Method for Measurement of Fracture Toughness," *Annual Book of ASTM Standards*, vol. 03.01, ASTM International, Conshohocken, PA, 2010.
6. ASTM Standard E466, "Practice for Conducting Force Controlled Constant Amplitude Axial Fatigue Tests of Metallic Materials," *Annual Book of ASTM Standards*, vol. 03.01, ASTM International, Conshohocken, PA, 2010.
7. A.D. Wilson, "Influence of Inclusions on the Fracture Properties of A588A Steel," *Fracture Mechanics: Fifteenth Symposium, ASTM STP 833*, American Society for Testing and Materials, Philadelphia, 1984, pp. 412-435.
8. H. Chen, G. Grondin and R.G. Driver, "Characterization of Fatigue Properties of ASTM A709 High Performance Steel," *J. Constructional Steel Research*, vol. 63, 2007, pp. 838-848.
9. R.L. Bodnar, F.B. Fletcher and M. Manohar, "The Physical Metallurgy of Normalized Plate Steels," *MS&T 2004 Conference Proceedings*, AIST, vol. 1, 2004, pp. 89-109.
10. J.D. Grozier and J.H. Bucher, "Correlation of Fatigue Limit with Microstructure and Composition of Ferrite-Pearlite Steels," *J. of Materials*, vol. 2, 1967, pp. 393-407.
11. K.J. Irvine and F.B. Pickering, "Low-Carbon Steels with Ferrite-Pearlite Structures," *JISI*, vol. 201, November 1963, pp. 944-959.
12. R.W. Hertzberg, *Deformation and Fracture Mechanics of Engineering Materials*, John Wiley & Sons, New York, 1976, p. 460.
13. K. Hussain and R.R. De Los Rios, "Microstructural Effect on Tensile and Fatigue Behavior of C-Mn Steel," *J. of Material Science*, vol. 32, 1997, pp. 3565-3569.
14. R.W. Landgraf, "Control of Fatigue Resistance Through Microstructure – Ferrous Alloys," in *Fatigue and Microstructure*, ASM, Metals Park, OH, 1979, pp. 453-455.
15. P. Watson and T.H. Topper, "An Evaluation of the Fatigue Performance of Automotive Steels," presented at the SAE Mid-Year Meeting, Montreal, June 7-11, 1971, Paper No. 710597.
16. T. Abe, T. Sampei, H. Osuzu and I. Kozasu, "Static Strengthening Mechanisms of Low and Medium Carbon Steels and Their Fatigue Strength," *Tetsu-to-Hagane*, vol. 70, no. 10, 1984, pp. 1459-1466.
17. R.L. Bodnar and S.S. Hansen, "Metallurgical Development of Rolled Steel Channels for Truck Frames," *32nd Mechanical Working & Steel Processing Conf. Proc.*, vol. XXVIII, 1991, pp. 61-72.